②

AD-A200 486

*SACLANT
RESEARCH
MEMORAN*

Detection of narrow-band
line-shaped signals
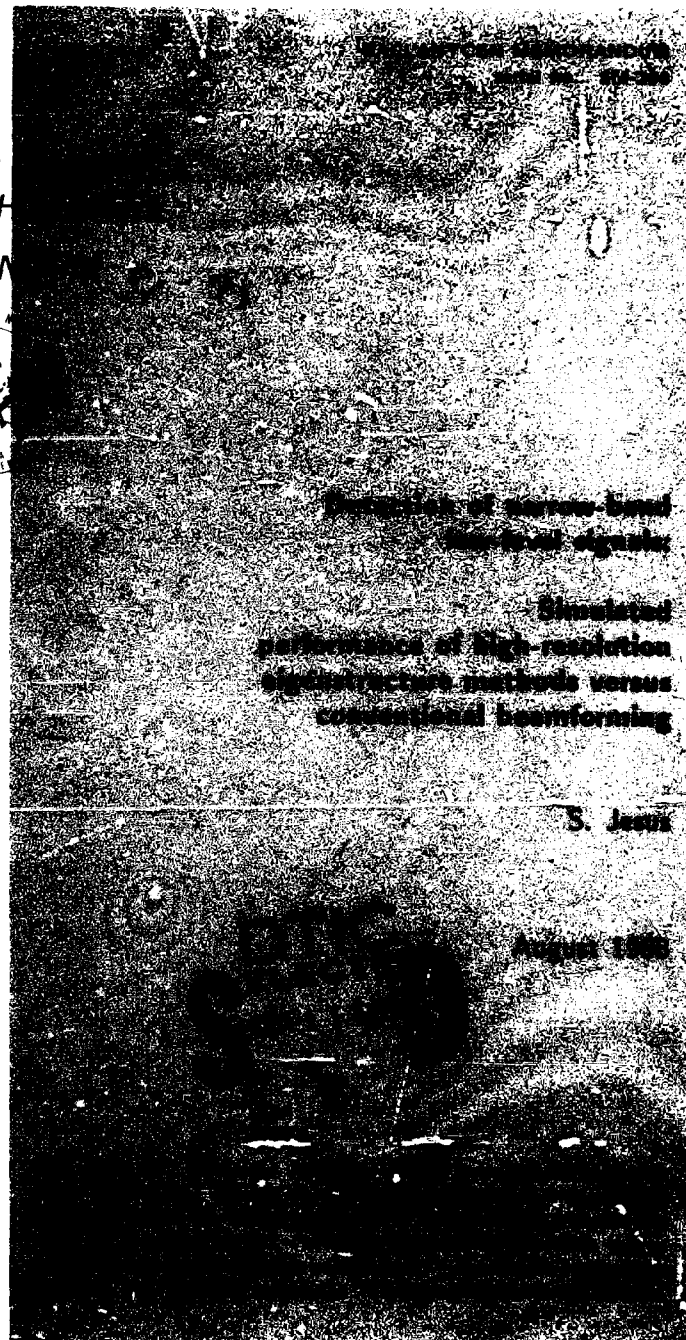
Simulated
performance of high-resolution
eigenstructure methods versus
conventional beamforming

S. Jauch

August 1988

Page count for SM-208
(excluding covers)

Pages	Total
i–vi	6
1–27	27
	33

SACLANT Undersea Research Centre
Viale San Bartolomeo 400
19026 San Bartolomeo (SP), Italy

tel: 0187 540 111
telex: 271148 SACENT I

NORTH ATLANTIC TREATY ORGANIZATION

Detection of narrow-band low-level signals:

Simulated performance of high-resolution eigenstructure methods versus conventional beamforming

S. Jesus

NTIS GRA&I ☒
DTIC TAB ☐
Unannounced ☐
Justification

By
Distribution/
Availability Codes

Dist	Avail and/or Special

A-1

Issued by:
Underwater Research Division

R. Thiele

R. Thiele
Division Chief

DTIC
SELECTED
OCT 1 1 1988
E

- ii -

intentionally blank page

Detection of narrow-band low-level signals:

Simulated performance of
high-resolution eigenstructure methods
versus conventional beamforming

S. Jesus

Executive Summary: In many instances, sonar performance and hence
ASW capability is limited by the sonar's spatial resolution, i.e. its ability
to separate acoustic signals arriving from close angles in order to obtain
both noise rejection and angle of arrival for the location and classification
of targets. This limitation is directly related to the length of the array, the
aperture.

In the last two decades a number of signal processing techniques have been
proposed that increase the resolution power of a given array without increas-
ing its length: these are the so-called high-resolution techniques. However,
although successful in other fields, their adoption in operational sonar sys-
tems has been slow. One reason for this is the difficulty in determining
the detection capability of high-resolution techniques compared with con-
ventional techniques, due to the absence of a commonly accepted measure
of performance that can be expressed in operational terms.

The aim of the present work is to improve this situation by showing, with
a simulation study, that the use of an appropriate high-resolution technique
may give a higher, and sometimes much higher, detection performance than
the conventional beamformer. Improvement can be obtained especially when
detecting a low-level target in the vicinity of one or more high-level interfer-
ing targets. This situation can occur in many crucial geographic areas where
the acoustic noise field is in major part due to the contribution of individual
ships behaving as interfering targets generating ship-induced noise fields.

The results of this work contribute to the understanding of the detection
behaviour of the high-resolution techniques in a number of realistic field
situations. Such techniques can also be viewed as an alternative to increas-
ing the array length and thereby improving the operational characteristics
of existing sonar systems. A companion report in preparation shows the
detection performance of these high-resolution techniques using real data.

Further progress requires improved knowledge of the background noise field,
its parametrisation in a noise model and its inclusion in the noise source es-
timation process as a priori information. The high-resolution techniques
presented here allow such information to be included. The results may sub-
stantially improve if this information is correct.

– iii –

intentionally blank page

Detection of narrow-band low-level signals:

Simulated performance of
high-resolution eigenstructure methods
versus conventional beamforming

S. Jesus

Abstract: In this report the detection of narrow-band low-level signals by passive sonar is addressed, specifically the detection of a low-level point source in a noise field modelled as a large number of high-level source lines embedded in white additive noise. This model may give, with a conventional processor, a measured noise field where the low-level source can be masked by high-level sources along similar directions. In this context, high-resolution eigenstructure detection algorithms are shown to achieve a significantly higher probability of detection than the conventional beamformer. The performance of four detection algorithms is compared using synthetic data – a companion report will present real data results.
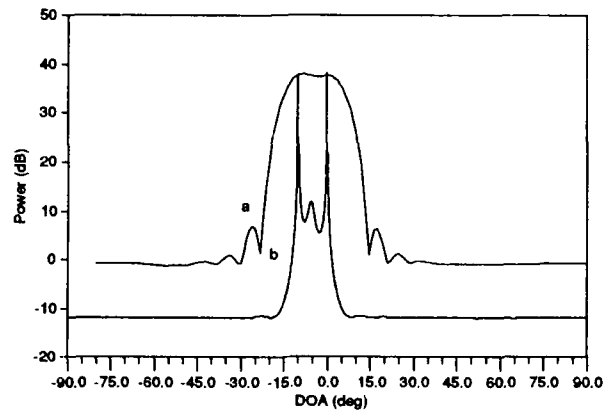
Fig. 1. Estimated power (dB) *vs* bearing (deg) – conventional beamformer with Hann shading (a) and high-resolution eigenstructure method (b): three sources at locations $-10°$, $-5°$ and $0°$; respective powers 30 dB, 0 dB and 30 dB; number of averages $N = 200$, 16 sensors.

Simulated tests have been conducted with different noise fields for variable relative location of the low-level source to the high-level interfering source(s), for variable signal-to-noise ratios, for different array shadings (conventional beamformer) and also for different observation times ('time–bandwidth products'). In a companion report [7] the methods described here are applied to real data and compared with previous results [6].

2. Background

Passive sonar target detection and classification is generally carried out by identifying the spectral content of a given data set with known ship and submarine acoustic spectral signatures. Source location is achieved by spatial processing to extract the directional features of the data. Time and space operations are generally performed separately. In this study we will concentrate on the spatial data processing for source detection and direction-of-arrival (DOA) estimation. Signals of interest are assumed to be of the narrow-band type for which the frequency bandwidth Δf is less than or equal to the frequency resolution $1/T_0$ of the fast fourier transform (FFT) used for spectrum estimation, $\Delta f \leq 1/T_0$.

2.1. DATA MODEL

The spatial field is sampled by a line array of L omnidirectional sensors at a constant interval d. To avoid spatial aliasing, d is assumed to be always $\leq c/2f_{max}$, where c is the sound speed and f_{max} is the highest frequency contained in the signal. Let $x_l(iT_s)$ be the lth sensor output at a discrete time iT_s where the sampling period T_s is chosen such that $T_s \leq 1/2f_{max}$. The signal $x_l(iT_s)$ is assumed to be stationary over a record length T_r. This interval T_r is then segmented into N equal intervals with $2K$ samples each, $T_r = 2NKT_s$. Each of the intervals is then passed through an FFT. Let

$$\mathbf{y}^T(n, f_k) = [y_1(n, f_k), y_2(n, f_k), \dots, y_L(n, f_k)], \qquad n = 1, \dots, N; k = 1, \dots, K, \tag{1}$$

be the L-dimensional array complex vector at time 'snapshot' n and for frequency f_k; T stands for the transpose. N is termed the 'time–bandwidth product', which is a compromise between data stationarity and power spectrum estimate stability. The spatial processing of $\mathbf{y}(n, f_k)$ will be achieved separately for each frequency f_k. Keeping this in mind, the frequency index will be omitted in the following for clarity.

The standard model to represent the observation vector $\mathbf{y}(n)$ with I far-field sources is [4]

$$\mathbf{y}(n) = \mathbf{A}\mathbf{s}(n) + \mathbf{v}(n). \tag{2}$$

Matrix $\mathbf{A}$ is an $L \times I$ complex matrix, the columns of which are the mode vectors

$$\mathbf{a}^T(\theta_i) = [1, e^{-j\nu_{\theta_i} d}, \dots, e^{-j(L-1)\nu_{\theta_i} d}], \qquad i = 1, \dots, I, \tag{3}$$

where the ith source wavenumber ν_{θ_i} is defined by

$$\nu_{\theta_i} = \frac{2\pi}{\lambda} \sin \theta_i$$

with λ being the source wavelength and θ_i the angle defined between the ith source wavefront and the normal to the array. In this case

$$\mathbf{A} = [\mathbf{a}(\theta_1), \mathbf{a}(\theta_2), \ldots, \mathbf{a}(\theta_I)]. \qquad (4)$$

In the standard model (2), the vector

$$\mathbf{s}(n) = [s_1(n), s_2(n), \ldots, s_I(n)] \qquad (5)$$

is the I-dimensional signal complex (analytic) vector where

$$s_i(n) = s_{ix}(n) + j s_{iy}(n), \qquad i = 1, \ldots, I. \qquad (5a)$$

The real and imaginary parts of $s_1(n)$ are assumed to be uncorrelated, stationary, and ergodic gaussian random processes with zero-mean and variance $\frac{1}{2}\sigma_{s_i}^2$. The covariance matrix of the signals is denoted

$$\mathbf{S} = E[s(\cdot)s(\cdot)^{\mathbf{H}}], \qquad (5b)$$

where H stands for the conjugate transpose.

Finally, the complex additive noise $\mathbf{v}(n)$ is assumed to be stationary, ergodic, zero-mean and with covariance

$$E[\mathbf{v}(\cdot)\mathbf{v}(\cdot)^{\mathbf{H}}] = \sigma_v^2 \mathbf{I}. \qquad (6)$$

where $\mathbf{I}$ is the identity matrix and σ_v^2 is a scalar representing the noise power. Moreover, the signals are assumed to be uncorrelated with the noise process.

In a DOA-estimation-only system, one uses the spectrum analyzer output data $\{\mathbf{y}(n); n = 1, \ldots N\}$ to estimate the set of angles $\{\theta_i; i = 1, \ldots, I\}$. The number of sources I is in general not known and also needs to be estimated. This problem, when the number of sources is not known, is often called a detection problem.

2.2. CONVENTIONAL BEAMFORMER

Only the case of a linear equispaced array will be treated. Conventional beamforming is a common nonparametric and computational efficient technique to combine the sensor outputs in this particular array arrangement. The computational efficiency of the conventional beamformer is mainly due to the use of a spatial, fourier transform implemented by the FFT algorithm [8].

The beamformer operates on the array by coherent summation of the L sensor outputs with the apropriate spatial delay to steer a 'beam' to a given direction θ. Let

$$b_n(\theta) = \sum_{l=1}^{L} h_l w_l(\theta) y_l(n) \tag{7}$$

be the complex beamformer output steered to direction θ at time 'snapshot' n. The term $w_l(\theta)$ contains the phase shift imposed to sensor l to steer the beamformer to direction θ,

$$w_l(\theta) = e^{j(l-1)\nu_\theta d}, \qquad l = 1, \ldots, L, \tag{8}$$

where all quantities have been defined above. The factor h_l is a spatial weight associated with sensor l; the sequence $\{h_l; l = 1, \ldots, L\}$ is known as the spatial shading function. The periodogram power wavenumber spectrum estimate is obtained by summing (7) over the N time segments, which gives for all beams

$$\widehat{\mathbf{B}}^N = \mathbf{W}'^H \widehat{\mathbf{R}}_{yy}^N \mathbf{W}', \tag{9}$$

where the matrix $\mathbf{W}'$ contains the direction vectors (8) weighted by the spatial function h_l. The matrix $\widehat{\mathbf{R}}_{yy}^N$ is a periodogram estimate of the data cross-covariance matrix $\mathbf{R}_{yy}$:

$$\widehat{\mathbf{R}}_{yy}^N = \frac{1}{N} \sum_{n=1}^{N} \mathbf{y}(n)\mathbf{y}^H(n). \tag{10}$$

2.3. HIGH-RESOLUTION EIGENSTRUCTURE METHOD

This method differs from the previous one mainly in the fact that it explicitly uses a model of the data-generating mechanism whereas the other did not. It provides much more accurate results if the model is appropriate. This parametrical method uses an interpretation of the measured data through time as a sequence of an L-dimensional vector moving in an L-dimensional vector space. If the array receives a certain number ($< L$) of coherent wavefronts the movement of the observed data vector is restricted to a certain linear subspace of the total L-dimensional reachable space. The method relies on the possibility of decomposing the total space into two linear subspaces: the signal subspace and the noise subspace.

3. Source detection

Source detection is a difficult problem in underwater passive listening due to the interrelation between the errors introduced by the technique used for array processing and the test of signal presence itself. Assuming the data model described in Subsect. 2.1 the optimal detector is

$$l_{\text{opt}}(\mathbf{y}) = \sigma_v^{-2} \mathbf{y}^H \mathbf{P} \mathbf{y}, \tag{20}$$

where $\mathbf{P}$ is the L-dimensional complex matrix

$$\mathbf{P} = (\sigma_v^2 \mathbf{I} + \mathbf{A} \mathbf{S} \mathbf{A}^H)^{-1} \mathbf{A} \mathbf{S} \mathbf{A}^H. \tag{21}$$

In practice, the detection characteristics of a receiving array are commonly described, in statistical terms, by the probabilities of detection (P_D) and of false alarm (P_{FA}) for a given signal-to-noise ratio (SNR). These two probabilities are respectively associated with the detection of a signal under the two hypotheses

H_1: signal plus noise is present, or

H_0: only noise is present.

Thus, the detection and false alarm probabilities are given by

$$P_D(\text{SNR}) = \text{Prob}\{l(\mathbf{y}) \geq \gamma(\text{SNR})/H_1\}, \tag{22a}$$

$$P_{FA}(\text{SNR}) = \text{Prob}\{l(\mathbf{y}) \geq \gamma(\text{SNR})/H_0\}. \tag{22b}$$

If $l(\mathbf{y})$ takes the form (20) the detection processor is said to be optimal (under the assumptions of the data model described in Subsect. 2 1).

3.1. WITH THE CONVENTIONAL BEAMFORMER

The standard scenario for testing hypothesis H_0/H_1 is to consider the possibility of presence of a single target in white additive noise. In this case, the received power estimate given by the beamformer (9) directed at the source location, say θ_1, is

$$\hat{B}^N(\theta_1)|_{H_0} = \dot{\sigma}_v^2, \tag{23a}$$

$$\hat{B}^N(\theta_1)|_{H_1} = \dot{\sigma}_{s_1}^2 + \dot{\sigma}_v^2. \tag{23b}$$

It can be proved that the conventional beamformer output (23) reaches, in this particular case, the optimal detector (20). Both (23a) and (23b) are χ^2 random distributed variables with $2N$ degrees of freedom and mean values σ_v^2 and $\sigma_{s_1}^2 + \sigma_v^2$ respectively. From the respective densities it is relatively easy to calculate the probability of detection P_D^0 for a fixed threshold B_T^0 depending on a given allowed fase alarm rate P_{FA}^0 (0 stands for zero interfering sources – see e.g. [9]).

Let us consider now the more realistic scenario of the detection of one low-level point source in the presence of a number of high-level interfering sources, all embedded in white additive noise. Assume I point sources at locations $\{\theta_i; i = 1, \ldots, I\}$. The beamformer is steered to the direction of the source we want to detect, say source 1 at bearing θ_1. The $I - 1$ interfering sources with powers $\{\sigma_{s_i}^2; i = 2, \ldots, I\}$ are located respectively at bearings $\{\theta_i; i = 2, \ldots, I\}$. Clearly using (9)

$$\hat{B}^N(\theta_1)|_{H_0} = \dot{\sigma}_v^2 + \sum_{i=2}^{I} \dot{\sigma}_{s_i}^2 \alpha_{1i}, \tag{24a}$$

$$\hat{B}^N(\theta_1)|_{H_1} = \dot{\sigma}_{s_1}^2 + \dot{\sigma}_v^2 + \sum_{i=2}^{I} \dot{\sigma}_{s_i}^2 \alpha_{1i}, \tag{24b}$$

where the last term represents, in both expressions, the sum of the 'influences' of the $I - 1$ interfering sources on estimating(and detecting) source 1. These 'influences' obviously depend on the relative location of source 1 to the interfering source(s). The factor α_{1i} is

$$\alpha_{1i} = \frac{1}{L^2} \left| \frac{\sin \frac{1}{2}\gamma_{1i}L}{\sin \frac{1}{2}\gamma_{1i}} \right|^2$$

with

$$\gamma_{1i} = \frac{2\pi f d}{c}(\sin \theta_1 - \sin \theta_i).$$

The detector given by (24) is no longer optimal. In effect, with some straightforward manipulations it can be shown that if at least one interference source is present, i.e. $\sum_{i=2}^{I} \sigma_{s_i}^2 \alpha_{1i} \neq 0$, then the probability of detection in the presence of interfering sources, P_D^I, is always less than or equal to the probability of detection with no

interfering sources, P_D^0 (for the same false alarm probability $P_{FA}^0 = P_{F*}^I$). This is, of course, due to the beampattern interference when detecting one source in a multi-source noise field. Let us recall that the sidelobe impact can be greatly reduced by using well-known techniques of sensor weighting (array shading). These techniques may improve the probability of detecting 'well-separated' sources with the counterpart of a loss in resolution and therefore a loss of detecting 'closely-separated' sources (within the beampattern mainlobe).

In conclusion, the degradation of the detection characteristics of the conventional beamformer is due to the array beampattern effect and is therefore related to the angular separation between sources and depends on their relative amplitude. We will show in Subsect. 3.2 that the detection characteristics of the high-resolution eigenstructure techniques do not suffer from any such inconveniences: they present a constant detection behaviour for all directions and in particular for low-level sources near to strong interfering sources.

3.2. WITH THE HIGH-RESOLUTION EIGENSTRUCTURE METHOD

Making use of the high-resolution eigenstructure method outlined in Subsect. 2.3, the problem of source detection is equivalent to the problem of estimating the dimension of the signal subspace $\mathbf{E_I}$ (17). The signal subspace dimension is equal to the number of highest non-equal eigenvalues of the cross-covariance matrix $\mathbf{R}_{yy}$ (12).

For a finite observation time, i.e. finite N, the eigenstructure of the estimated cross-covariance matrix $\widehat{\mathbf{R}}_{yy}^N$ (10) based on the observation set (1) is defined by

$$\widehat{\mathbf{R}}_{yy}^N \hat{\mathbf{e}}_l = \hat{\lambda}_l \hat{\mathbf{e}}_l, \qquad l = 1, \ldots, L. \tag{25}$$

The estimated eigenvalues

$$\hat{\lambda}_1 \geq \hat{\lambda}_2 \geq \ldots \geq \hat{\lambda}_l \geq \ldots \geq \hat{\lambda}_L \geq 0. \tag{26}$$

are all different with probability one [10] making it difficult to find the number of signals by merely 'looking' at the eigenvalue distribution.

Two approaches have been proposed to solve this problem - the generalized likelihood ratio test [11] and the information-based theoretic criteria [12]:

- The first approach splits the decision problem into a sequence of yes/no answers to a series of questions: 'Is the number of sources equal to k for $k = 0, \ldots, L - 1$?' Under the hypothesis-testing theory, answering 'yes' to the question is equivalent to accepting the hypothesis

$$\mathbf{H}_k: \text{ there are at most } k \text{ sources}$$

Answering 'no' is equivalent to accepting $\overline{H}_k$:

$\overline{H}_k$: there are at least $k + 1$ sources.

Starting with $k = 0$ the test is performed until $\overline{H}_k$ is rejected (equivalent to accepting H_k) or $k = L - 1$, in which case $\hat{k} = L$.

- The second approach treats the decision problem as the determination of the rank of the signal matrix which is considered as a model selection problem. The selected model is the one that 'best' fits the data under certain criteria. Two methods for this approach have been proposed: the Akaike information criteria (AIC) and the minimum descriptor length (MDL).

All three methods referred to above are ultimately seeking to test for the equality of the $L - k$ smallest eigenvalues of the sample cross-covariance matrix. This test is known in the literature as 'the sphericity test' [13,14].

The assumption that the data is a series of zero-mean statistically independent gaussian random vectors leads to an optimum estimation of the model parameters provided by the maximum likelihood estimator. It is well known that in this case the functional

$$T(k) = -2\log\alpha_k, \tag{27}$$

where α_k is the likelihood ratio given by

$$\alpha_k = \left(\frac{\prod_{i=k+1}^{L} \hat{\lambda}_i^{1/(L-k)}}{(L-k)^{-1}\sum_{i=k+1}^{L}\hat{\lambda}_i} \right)^{(L-k)}, \tag{28}$$

is distributed for large samples approximately as χ^2 [15,16]. This statistic is used by the three criteria, the difference being only in the modifications used to approximate the asymptotical χ^2 distribution for short or moderate sample size. We are not attempting to derive the whole underlying theory as this has already been extensively covered in the literature referred to above; only the expressions for the criteria are given below.

Generalized likelihood ratio test (GLRT)   Following Liggett [11] a corrected test for moderate sample size would be

$$T_{\text{GLRT}}(k) = \mu(k)\log\alpha_k \tag{29}$$

with the multiplying factor $\mu(k)$ equal to

$$\mu(k) = \frac{-2(N - k - \{2(L - k)^2 + 1\})}{6(L - k)} \tag{30}$$

This test is conducted until

$$T_{\text{GLRT}}(k) > t_0^k \tag{31}$$

- 11 -

or $k = L - 1$. The detection threshold t_0^k is drawn from a $\chi^2_{\nu_k}$ distribution with $\nu_k = (L - k)^2 - 1$ degrees of freedom for a given significance η_k fixed by the operator such that

$$\text{Prob}\{\chi^2_{\nu_k} \geq t_0^k\} = \eta_k. \tag{32}$$

Akaike Information Criteria (AIC)   From [12], the estimated number of signals is, according to the AIC criteria, the value of $k = 0, \ldots, L - 1$ for which

$$T_{\text{AIC}}(k) = -2N \log \alpha_k + 2k(2L - k) \tag{33}$$

is minimum.

Minimum Descriptor Length (MDL)   Also from [12], the number of signals is equal to the value of $k = 0, \ldots, L - 1$ that minimizes the functional

$$T_{\text{MDL}}(k) = -N \log \alpha_k + \tfrac{1}{2}k(2L - k) \log N. \tag{34}$$

Comparing these detection procedures, the first remark is that they are obviously independent of the relative location of the sources, in contrast to the conventional beamformer. They depend only on the observation time or equivalently on the number of samples N. This is the well-known behaviour of the high-resolution eigenstructure techniques which have asymptotic (large N) infinite resolving power [5]. This will be clearly illustrated in Sect. 4 by simulation.

4. Simulation results

For each case the probabilities of detection are estimated as a function of the input signal-to-noise ratio (SNR_{in}) and the relative location (DOA_r) of the low-level source to the high-level interfering source(s). Two simulated noise fields were generated to illustrate the comparative behaviour of the four detection algorithms. In the first example the noise field is formed by two line sources in a flat background noise: one is the high-level interfering source which is fixed in location and in power and the other is the low-level source on which the detection is performed. In the second example the low-level source is located between two high-level sources, having a fixed power but a variable angular separation. The data has been generated according to model (2) with the parameters given in Table 1. In both examples two 'time–bandwidth products' were tested. Also two array shadings were used in the conventional beamformer: uniform and Hann shading. For each case four curves are plotted corresponding to the four detection algorithms being tested:

- Conventional beamformer (CVB – curve C).

- Akaike information criteria (AIC – curve A).

- Minimum descriptor length (MDL – curve M).

- Generalized likelihood ratio test (GLRT – curve G).

4.1. EXAMPLE 1: ONE HIGH-LEVEL INTERFERING SOURCE

The empirical detection characteristics are shown in Figs. 2 to 5. The probability of detection, for a constant false alarm probability, is given *vs* the input signal-to-noise ratio in Fig. 2 and *vs* the relative location in Figs. 3 to 5. The probability of false alarm can be controlled in the conventional beamformer but not in the other detection algorithms. In this example, the empirical estimation of the false alarm rate over 000 statistically independent draws gave the results shown in Table 2. Among the three high-resolution detection algorithms one can note that while the AIC algorithm provides the largest probability of false alarm (2.7%), the probability of false alarm of the MDL algorithm could not be evaluated with this sample size. The mean P_{FA} of all three high-resolution algorithms is about 1%, which is aproximately the value for the conventional beamformer; therefore the true comparable characteristics are relatively close to the curves shown.

Comments   Observing Fig. 2, one can remark that the CVB performs better than all the other algorithms for $DOA_r = -30°$ (a), its performance then gradually decreases when approaching the high-level source (b) and (c), and is null for $DOA_r =$
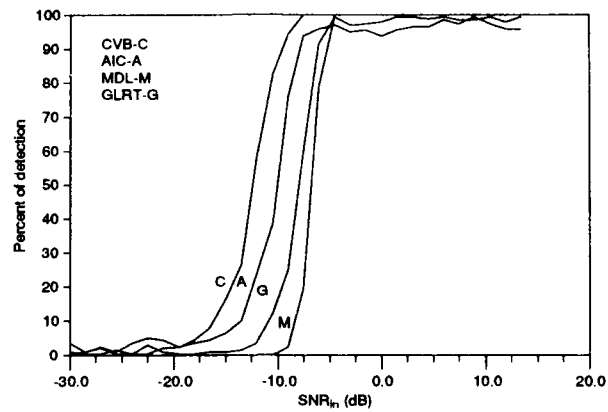
Fig. 2a. Estimated probability of detection (%) *vs* the input signal-to-noise ratio (dB), one interfering source at $-10°$, $N = 50$, $N_D = 200$, Hann weighting $DOA_r = -30°$.
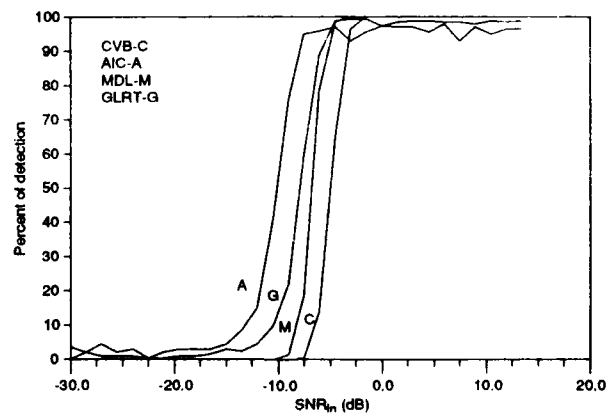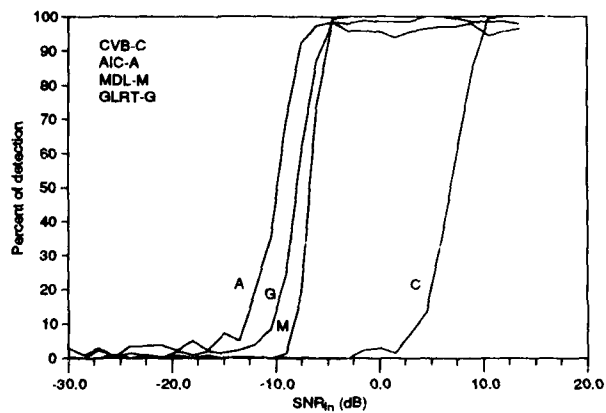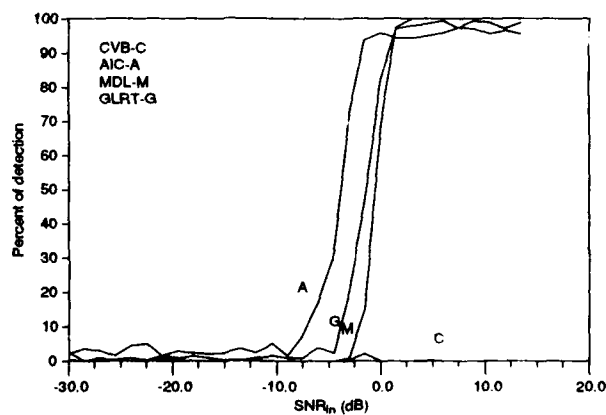

Fig. 2b. Estimated probability of detection (%) *vs* the input signal-to-noise ratio (dB), one interfering source at $10°$, $N = 50$, $N_D = 200$, Hann weighting $DOA_r = -18°$.

- 14 -

Fig. 2c. Estimated probability of detection (%) *vs* the input signal-to-noise ratio (dB), one interfering source at 10°. $N = 50$, $N_D = 200$, Hann weighting DOA$_r = -10°$.

Fig. 2d. Estimated probability of detection (%) *vs* the input signal-to-noise ratio (dB), one interfering source at 10° $N = 50$. $N_D = 200$, Hann weighting DOA$_r = 2°$

Table 1
Input parameters for the simulated tests

Parameter	Symbol	Value	Fig. no.
number of statistical draws	N_D	200	2–9
number of hydrophones	L	16	2–9
spacing/wavelength	d/λ	0.5	2–9
noise power (dB)	σ_v^2	0	2–9
time–bandwidth product	N	$\begin{cases} 50 \\ 200 \end{cases}$	2–4,6–8 / 5,9
array shading (CVB)		$\begin{cases} \text{Hann} \\ \text{uniform} \end{cases}$	2,3,5–9 / 4
Example 1			
number of signals	I	2	2–5
signal-to-noise ratio (dB)	$\begin{cases} \sigma_1^2/\sigma_v^2 \\ \sigma_2^2/\sigma_v^2 \end{cases}$	$\in [-20,13.5]$ / 30	2–5 / 2–5
signal location (deg)	$\begin{cases} \text{DOA}_1 \\ \text{DOA}_2 \end{cases}$	$\in [-20,9]$ / 10	2–5 / 2–5
Example 2			
number of signals	I	3	6–9
signal-to-noise ratio (dB)	$\begin{cases} \sigma_1^2/\sigma_v^2 \\ \sigma_2^2/\sigma_v^2 \\ \sigma_3^2/\sigma_v^2 \end{cases}$	5,10,15 / 30 / 30	6–9 / 6–9 / 6–9
signal location (deg)	$\begin{cases} \text{DOA}_1 \\ \text{DOA}_2 \\ \text{DOA}_3 \\ \text{DOA}_3 \end{cases}$	$\in [\text{DOA}_2,\text{DOA}_3]$ / -10 / $-5,0,5$ / -5	6–9 / 6–9 / 6–8 / 9

Table 2
Empirical probability of false alarm, Example 1

Algorithm	P_{FA} (%)
CVB	1.1
AIC	2.7
MDL	0.0
GLRT	0.7

$-2°$ (d). For the same bearing variation the performance of the high-resolution algorithms is relatively constant, unless for case (d) where a slight decrease of about 2.5 dB can be noted.

In Fig. 3 the improvement obtained by the high-resolution algorithms is clearly seen in terms of source location. As expected, the CVB performance is always better than that of the other algorithms when the source is far away from the interfering source. However, for a low-level source with $SNR_{in} = -6$ dB (a) the sidelobe decreases the CVB performance 19° away from the interference location. Figure 3b shows a similar behaviour for an $SNR_{in} = 0$ dB: in this figure the influence of the mainlobe appears for $|DOA_r| < 12°$.

In Fig. 4 the conventional beamformer performance is shown with uniform shading instead of Hann shading. Only one signal-to-noise ratio is shown: $SNR_{in} = 5$ dB. As expected, the detection performance curve of the conventional beamformer has a spikey aspect which is directly related with the high-level source beampattern: the maxima of detection corresponding to the nulls and the minima of detection to the peaks of the beampattern. The main difference, compared to the Hann shading results, is the fact that large losses of detection can be obtained even for directions 'far away' from the interference direction.

In Fig. 5 the 'time–bandwidth product' was increased to $N = 200$. The conventional beamformer performance (with Hann shading) is approximately the same while the high-resolution algorithms behave significantly better.

4.2. EXAMPLE 2: TWO HIGH-LEVEL INTERFERING SOURCES

The results of this test are shown in Figs. 6 to 9. In these figures the percentage of detection probability is given vs the relative location of the low-level source to the fixed high-level source normalized by the separation of the two high-level sources. The fixed high-level source is located at $DOA_{i1} = -10°$. The separation of the two high-level sources, ΔDOA_i, is variable and takes the following values: 5° (Figs. 6 and 9), 10° (Fig. 7) and 15° (Fig. 8). Thus, the normalized DOA_n is given by

$$DOA_n = \frac{DOA_s - DOA_{i1}}{\Delta DOA_i},$$

where DOA_s is the location of the signal under detection.

An empirical estimation of the false alarm rate for the four algorithms gave the results summarized in Table 3. One can note that the overall P_{FA} decreased in this test and is now situated around 0.7%.
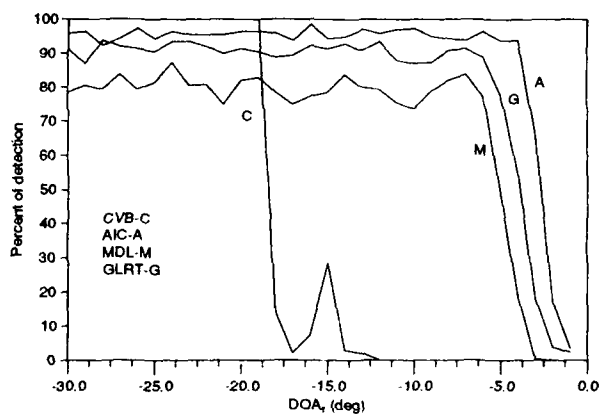
Fig. 3a. Estimated probability of detection (%) vs the relative location to the interfering source at $-10°$, $N = 50$, $N_D = 200$, Hann weighting $SNR_{in} = -6$ dB.
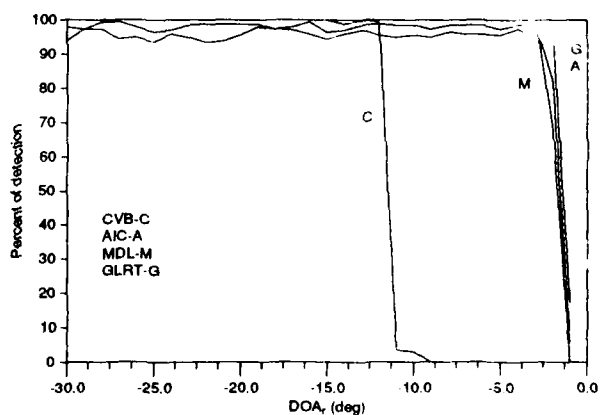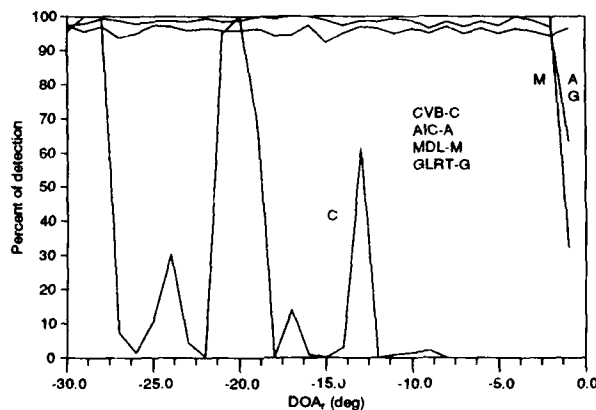

Fig. 3b. Estimated probability of detection (%) vs the relative location to the interfering source at $10°$ N 50, N_D 200. Hann weighting $SNR_{in} = 0$ dB.

Fig. 4. Estimated probability of detection (%) *vs* the relative location to the interfering source at $-10°$, $N = 50$, $N_D = 200$, uniform weighting $SNR_{in} = 5$ dB.

Comments Figures 6 through 9 show a similar behaviour: the high-resolution algorithms could achieve some detections (and in some cases a good detection rate) whereas the conventional beamformer did none. As expected, from the results of Example 1, higher detection probabilities where obtained for larger SNR's, for larger separations betwwen the two high-level sources and with maxima at the half-separation of the interfering sources. Also, as before, a larger number of averages improves the results of the high-resolution techniques (Fig. 9).

Table 3
Empirical probability of false alarm, Example 2

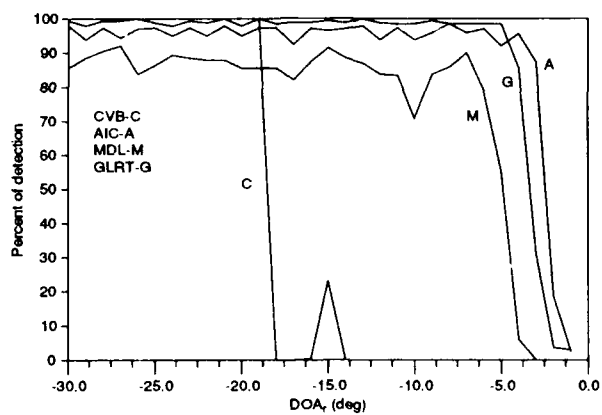| Algorithm	P_{FA} (%)
CVB	0.6
AIC	1.8
MDL	0.0
GLRT	0.6

- 19 -

Fig. 5a. Estimated probability of detection (%) *vs* the relative location to the interfering source at $-10°$, $N = 200$, $N_D = 200$, Hann weighting $SNR_{in} = -9$ dB.
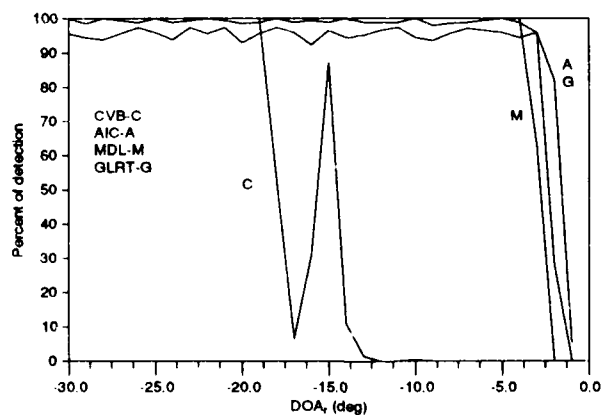

Fig. 5b. Estimated probability of detection (%) *vs* the relative location to the interfering source at $-10°$, $N = 200$, $N_D = 200$, Hann weighting $SNR_{in} = -6$ dB.
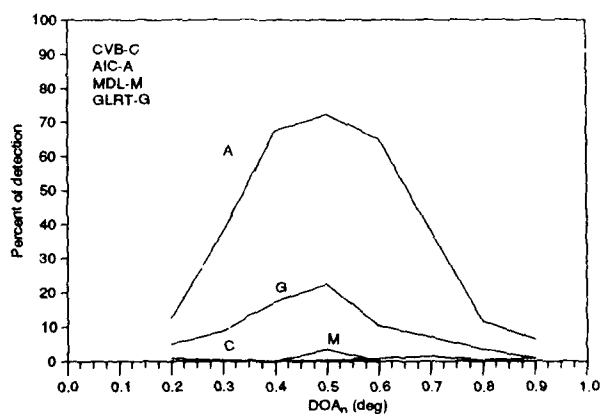
- 20 -

Fig. 6a. Estimated probability of detection (%) *vs* the normalized relative location to the two interfering sources at $-10°$ and $-5°$, $N = 50$, $N_D = 200$, Hann weighting $SNR_{in} = 5$ dB.
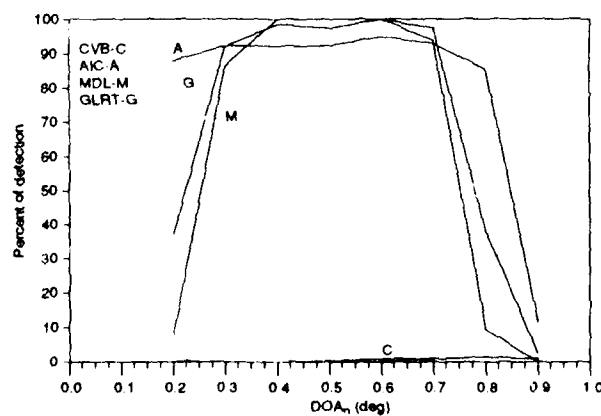

Fig. 6b. Estimated probability of detection (%) *vs* the normalized relative location to the two interfering sources at $-10°$ and $-5°$, $N = 50$, $N_D = 200$, Hann weighting $SNR_{in} = 10$ dB.

21 -

Fig. 7a. Estimated probability of detection (%) *vs* the normalized
relative location to the two   rfering sources at −10° and 0°,
$N = 50$, $N_D = 200$, Hann weighting $SNR_{in} = -5$ dB.

Fig. 7b. Estimated probability of detection (%) *vs* the normalized
relative location to the two interfering sources at −10° and 0°,
$N = 50$, $N_D = 200$, Hann weighting $SNR_{in} = 0$ dB.

Fig. 8a. Estimated probability of detection (%) *vs* the normalized relative location to the two interfering sources at $-10°$ and $5°$, $N = 50$, $N_D = 200$, Hann weighting $SNR_{in} = -10$ dB.
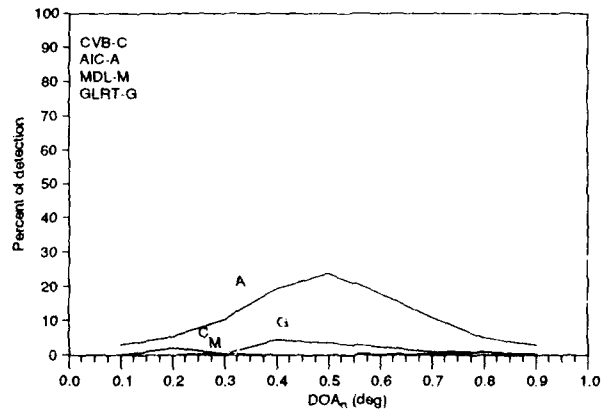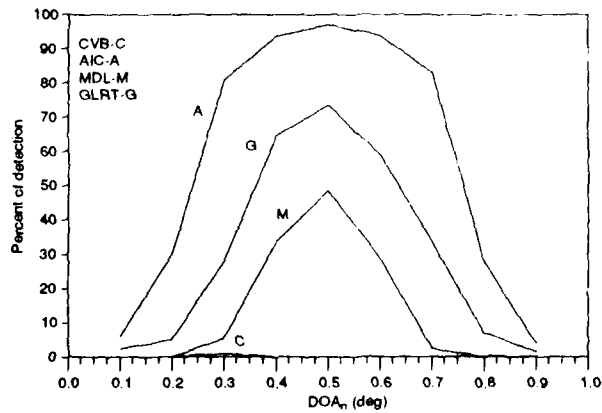

Fig. 8b. Estimated probability of detection (%) *vs* the normalized relative location to the two interfering sources at $-10°$ and $5°$, $N = 50$, $N_D = 200$, Hann weighting $SNR_{in} = -5$ dB.

23

Fig. 9a. Estimated probability of detection (%) vs the normalized relative location to the two interfering sources at $-10°$ and $-5°$, $N = 200$, $N_D = 200$, Hann weighting $SNR_{in} = 0$ dB.
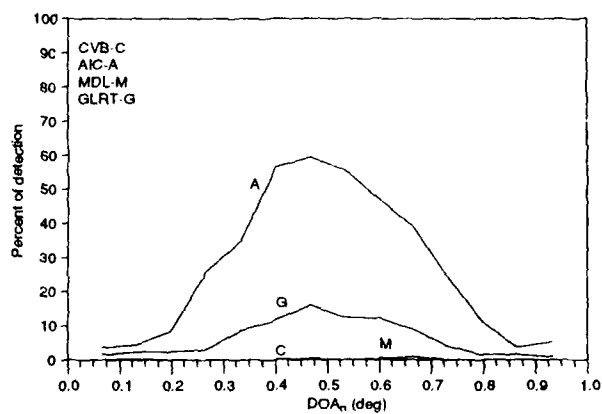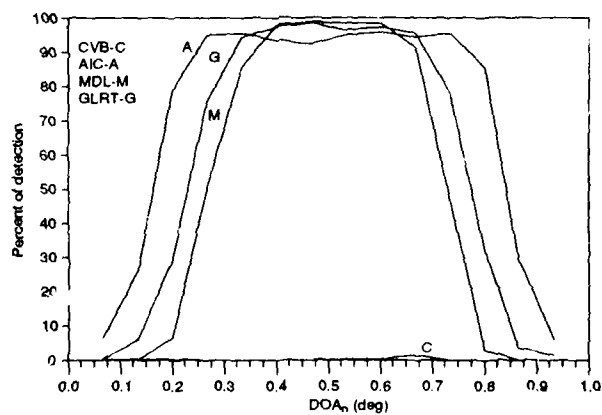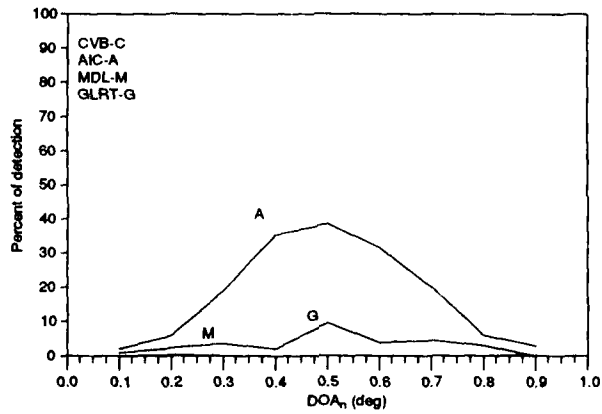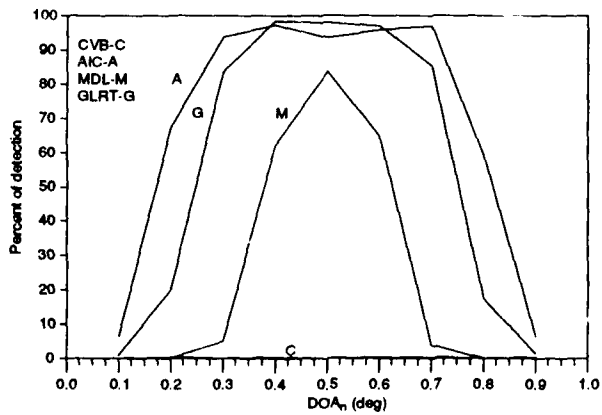

Fig. 9b. Estimated probability of detection (%) vs the normalized relative location to the two interfering sources at $-10°$ and $-5°$, $N = 200$, $N_D = 200$, Hann weighting $SNR_{in} = 5$ dB.

5. Conclusion

The problem of detecting a low-level source in the presence of high-level interfering sources has been studied in this report using simulated data. The performance of the conventional beamformer has been compared with three high-resolution beamformers based on eigenstructure decomposition techniques. From the simulations it has been possible to estimate the probability of detection of the low-level source keeping the probability of false alarm approximately constant. As expected, the simulation shows that the conventional beamformer performance, although optimal in a single-source scenario, is greatly reduced when attempting to detect a low-level source near to high-level interfering sources.

The detection performance of the high-resolution algorithms is significantly better than that of the conventional beamformer for a low-level source located within the mainlobe of a high-level interfering source. When more than one high-level source is present the performance improvement can be extremely high. In the case of a *very* low-level source the high-resolution techniques can achieve a detection improvement even in the sidelobe region. The detection behaviour of the high-resolution techniques is relatively constant in bearing except for the interference direction; this behaviour is improved by a longer observation time.

Among the three high-resolution detection algorithms, AIC always displayed the best performance – together with the highest false alarm rate – and MDL displayed the best results – together with the lowest false alarm rate. This is in agreement with the asymptotical consistency remarked by [12,17].

In conclusion, the results suggest that the high-resolution algorithms can achieve a real improvement in detecting low-level targets in ship-induced noise fields. A disadvantage of the high-resolution algorithms is their dependence on a knowledge of the noise field Deviations from the assumed noise field, which may occur in real data, can lead to a degradation in detection performance. In a companion report [7] we present real data-processing results which show the robustness of the high-resolution detection algorithms.

References

[1] CAPON, J. High-resolution frequency-wavenumber spectrum analysis. *Proceedings of the IEEE*, **57**, 1969: 1408–1418.

[2] BURG, J.P. Maximum entropy spectral analysis. PhD. Dissertation. Stanford University, 1975.

[3] PISARENKO, V.F. The retrieval of harmonics from a covariance function. *Geophysical Journal of the Royal Astronomical Society*, **33**, 1973: 347–366.

[4] SCHMIDT, R.O. A signal subspace approach to multiple emitter location and spectral estimation. PhD. Dissertation. Stanford University, 1982.

[5] BIENVENU, G. Influence of the spatial coherence of the background noise on high resolution passive methods. *In*: INSTITUTE OF ELECTRICAL AND ELECTRONICS ENGINEERS. ACOUSTICS SPEECH AND SIGNAL PROCESSING SOCIETY. *ed.* International Conference on Acoustics, Speech and Signal Processing. Washington, D.C., 2–4 April, 1979: pp. 306–309.

[6] JESUS, S. and HEITMEYER, R.M. Results on the detection of narrow-band low-level signals in a ship-induced noise field using high-resolution beamforming. In preparation as a SACLANTCEN document.

[7] JESUS, S. Passive sonar: low-frequency target detection in ship-induced noise fields using high-resolution eigenstructure techniques. In preparation as a SACLANTCEN document.

[8] WILLIAMS, J.R. Fast beam-formimg algorithm. *Journal of the Acoustical Society of America*, **44**, 1968: 1454–1455.

[9] WONG, K.M. and CHEN, S. Detection of narrow-band sonar signals using order statistical filters. *IEEE Transactions on Acoustics, Speech and Signal Processing*, **35**, 1987: 597–612.

[10] ANDERSON, T.W. An Introduction to Multivariate Statistical Analysis. New York, NY, Wiley, 1958.

[11] LIGGETT, Jr., W.S. Passive sonar: fitting models to multiple time series. *In*: GRIFFITHS, J.W.R. and STOCKLIN, P.L., *eds.* Proccedings of the NATO Advanced Study Institute on Signal Processing with Particular Reference to Underwater Acoustics, Loughborough, 21 August to 1 September, 1972. London, Academic Press, 1973: pp. 327–345.

[12] WAX, M. and KAILATH, T. Detection of signals by information theoretic criteria. *IEEE Transactions on Acoustics, Speech and Signal Processing*, vol. ASSP-33, **2**, 1985: 387–392.

[13] ANDERSON, T.W. Assymptotic theory for principal component analysis. *Annals of Mathematical Statistics*, **34**, 1963: 122–148.

[14] JAMES, A.T. Tests of equality of latent roots of the covariance matrix. *In*: KRISHNAIAH, P.R. *ed.* Multivariate Analysis II, New York, NY, Academic Press, 1969: pp. 205–218.

[15] WILKS, S.S. The large sample distribution of the likelihood ratio for testing composite hypothesis. *Annals of Mathematical Statistics*, 1938: 60.

[16] LAWLEY, D.N. A general method for approximating to the distribution of likelihood ratio criteria. *Biometrika*, **43**, 1956: 295–303.

[1.] ZHAO, L., KRISHNAIAH, P.R. and BAI, Z. Remarks on certain criteria for detection of number of signals. *IEEE Transactions on Acoustics, Speech and Signal Processing*, **35**, 1987: 129–132.

Initial Distribution for SM-208

Ministries of Defence			NR Germany	1
JSPHQ Belgium	2		CNR Greece	1
DND Canada	10		CNR Italy	1
CHOD Denmark	8		SCNR Netherlands	1
MOD France	8		SCNR Norway	1
MOD Germany	15		SCNR Portugal	1
MOD Greece	11		SCNR Turkey	1
MOD Italy	10		SCNR UK	1
MOD Netherlands	12		SCNR US	2
CHOD Norway	10		French Delegate	1
MOD Portugal	2		SECGEN Rep. SCNR	1
MOD Spain	2		NAMILCOM Rep. SCNR	1
MOD Turkey	5		National Liaison Officers	
MOD UK	20		NLO Canada	1
SECDEF US	68		NLO Denmark	1
			NLO Germany	1
NATO Authorities			NLO Italy	1
Defence Planning Committee	3		NLO UK	1
NAMILCOM	2		NLO US	1
SACLANT	3			
SACLANTREPEUR	1		NLR to SACLANT	
CINCWESTLANT/			NLR Belgium	1
COMOCEANLANT	1		NLR Canada	1
COMSTRIKFLTANT	1		NLR Denmark	1
CINCIBERLANT	1		NLR Germany	1
CINCEASTLANT	1		NLR Greece	1
COMSUBACLANT	1		NLR Italy	1
COMMAIREASTLANT	1		NLR Netherlands	1
SACEUR	2		NLR Norway	1
CINCNORTH	1		NLR Portugal	1
CINCSOUTH	1		NLR Turkey	1
COMNAVSOUTH	1		NLR UK	1
COMSTRIKFORSOUTH	1			
COMEDCENT	1			
COMMARAIRMED	1			
CINCHAN	3			
			Total external distribution	250
SCNR for SACLANTCEN			SACLANTCEN Library	10
SCNR Belgium	1		Stock	20
SCNR Canada	1			
SCNR Denmark	1		Total number of copies	280

END

DATE
FILMED

1-88